arXiv:1009.0344v2 [astro-ph.SR] 25 Apr 2012

OGLE-2005-BLG-153: MICROLENSING DISCOVERY AND CHARACTERIZATION OF A VERY LOW MASS BINARY

K.-H. HWANG[1], A. UDALSKI[2], C. HAN[1,39], Y.-H. RYU[1], I.A. BOND[4], J.-P. BEAULIEU[5], M. DOMINIK[6], K. HORNE[6], A. GOULD[7], B.S. GAUDI[7]

AND

M. KUBIAK[2], M.K. SZYMAŃSKI[2], G. PIETRZYŃSKI[2,8], I. SOSZYŃSKI[2], O. SZEWCZYK[2,8], K. ULACZYK[2], Ł. WYRZYKOWSKI[2,9]
(THE OGLE COLLABORATION),
F. ABE[10], C.S. BOTZLER[12], J.B. HEARNSHAW[13], Y. ITOW[10], K. KAMIYA[10], P.M. KILMARTIN[14], K. MASUDA[10], Y. MATSUBARA[10], M. MOTOMURA[10], Y. MURAKI[16], S. NAKAMURA[10], K. OHNISHI[17], C. OKADA[10], N. RATTENBURY[12], To. SAITO[18], T. SAKO[10], M. SASAKI[10], D.J. SULLIVAN[15], T. SUMI[10], P.J. TRISTRAM[15], J.N. WOOD[12], P.C.M. YOCK[12], T. YOSHIOKA[10]
(THE MOA COLLABORATION),
M. ALBROW[26], D.P. BENNETT[11], D.M. BRAMICH[19], S. BRILLANT[24], J.A.R. CALDWELL[35], J.J. CALITZ[36], K.H. COOK[37], E. CORRALES[5], C. COUTURES[20], M. DESORT[5], S. DIETERS[22], D. DOMINIS[21], J. DONATOWICZ[19] P. FOUQUÉ[27], J. GREENHILL[22], K. HARPSØE[23,38], K. HILL[22], M. HOFFMAN[21], U.G. JØRGENSEN[23,38], S. KANE[28], D. KUBAS[5], R. MARTIN[25], J.-B. MARQUETTE[5], P. MEINTJES[36], J. MENZIES[29], K. POLLARD[26], K. SAHU[30], I. STEELE[32], C. VINTER[23], J. WAMBSGANSS[31], A. WILLIAMS[25], K. WOLLER[23], M. BURGDORF[32], C. SNODGRASS[33], M. BODE[32]
(THE PLANET/ROBONET COLLABORATION);
AND
D.L. DEPOY[34], C.-U. LEE[3], B.-G. PARK[3], R.W. POGGE[7] (THE μFUN COLLABORATION)
Draft version June 8, 2018

ABSTRACT

The mass function and statistics of binaries provide important diagnostics of the star formation process. Despite this importance, the mass function at low masses remains poorly known due to observational difficulties caused by the faintness of the objects. Here we report the microlensing discovery and characterization of a binary lens composed of very low-mass stars just above the hydrogen-burning limit. From the combined measurements of the Einstein radius and microlens parallax, we measure the masses of the binary components of $0.10 \pm 0.01\,M_\odot$ and $0.09 \pm 0.01\,M_\odot$. This discovery demonstrates that microlensing will provide a method to measure the mass function of all Galactic populations of very low mass binaries that is independent of the biases caused by the luminosity of the population.

1. INTRODUCTION

1

[1] Department of Physics, Chungbuk National University, Cheongju 361-763, Republic of Korea.

[2] Warsaw University Observatory, Al. Ujazdowskie 4, 00-478 Warszawa, Poland.

[3] Korea Astronomy and Space Science Institute, Daejeon 305-348, Republic of Korea.

[4] Institute of Information and Mathematical Sciences, Massey University, Private Bag 102-904, North Shore Mail Centre, Auckland, New Zealand.

[5] Institut d'Astrophysique de Paris, CNRS, Université Pierre et Marie Curie UMR7095, 98bis Boulevard Arago, 75014 Paris, France.

[6] Scottish Universities Physics Alliance, University of St Andrews, School of Physics and Astronomy, North Haugh, St Andrews KY16 9SS, UK.

[7] Department of Astronomy, The Ohio State University, 140 W. 18th Ave., Columbus, OH 43210, USA.

[8] Universidad de Concepción, Departamento de Fisica, Casilla 160-C, Concepción, Chile.

[9] Institute of Astronomy, University of Cambridge, Madingley Road, Cambridge CB3 0HA, UK.

[10] Solar-Terrestrial Environment Laboratory, Nagoya University, Nagoya, 464-8601, Japan.

[11] Department of Physics, University of Notre Dame, Notre Dame, IN 46556, USA.

[12] Department of Physics, University of Auckland, Private Bag 92019, Auckland, New Zealand.

[13] University of Canterbury, Department of Physics and Astronomy, Private Bag 4800, Christchurch 8020, New Zealand.

[14] Mt. John Observatory, P.O. Box 56, Lake Tekapo 8770, New Zealand.

[15] School of Chemical and Physical Sciences, Victoria University, Wellington, New Zealand.

[16] Department of Physics, Konan University, Nishiokamoto 8-9-1, Kobe 658-8501, Japan.

[17] Nagano National College of Technology, Nagano 381-8550, Japan.

[18] Tokyo Metropolitan College of Industrial Technology, Tokyo 116-8523, Japan.

[19] European Southern Observatory, Karl-Schwarzschild-Straβe 2, 85748 Garching bei München, Germany.

[20] CEA DAPNIA/SPP Saclay, 91191 Gif-sur-Yvette cedex, France.

[21] Universität Potsdam, Institut für Physik, Am Neuen Palais 10, 14469 Potsdam, Astrophysikalisches Institut Potsdam, An der Sternwarte 16, D-14482, Potsdam, Germany.

[22] University of Tasmania, School of Mathematics and Physics, Private Bag 37, Hobart, TAS 7001, Australia.

[23] Niels Bohr Institute, University of Copenhagen, Juliane Maries Vej 30, 2100 Copenhagen, Denmark.

[24] European Southern Observatory, Casilla 19001, Santiago 19, Chile.

[25] Perth Observatory, Walnut Road, Bickley, Perth, WA 6076, Australia.

[26] University of Canterbury, Department of Physics and Astronomy, Private Bag 4800, Christchurch 8020, New Zealand.

[27] Observatoire Midi-Pyrénées, Laboratoire d'Astrophysique, UMR 5572, Université Paul Sabatier-Toulouse 3, 14 avenue Edouard Belin, 31400 Toulouse, France.

[28] Department of Astronomy, University of Florida, 211 Bryant Space Science Center, Gainesville, Florida 32611-2055, USA.

[29] South African Astronomical Observatory, PO Box 9, Observatory 7935, South Africa.

[30] Space Telescope Science Institute, 3700 San Martin Drive, Baltimore, Maryland 21218, USA.

[31] Astronomisches Rechen-Institut (ARI), Zentrum für Astronomie, Universität Heidelberg, Mönchhofstrasse 12-14, 69120 Heidelberg, Germany.

[32] Astrophysics Research Institute, Liverpool John Moores University, Twelve Quays House, Egerton Wharf, Birkenhead CH41 1LD, UK.

[33] Max Planck Institute for Solar System Research, Max-Planck-Str. 2, 37191 Katlenburg-Lindau, Germany.

[34] Department of Physics, Texas A&M University, College Station, TX, USA.

[35] McDonald Observatory, 16120 St Hwy Spur 78 #2, Fort Davis, Texas 79734, USA

[36] Boyden Observatory, University of the Free State, Department of Physics,

2. INTRODUCTION

Microlensing occurs when a foreground astronomical object (lens) is closely aligned to a background star (source) and the light from the source star is deflected by the gravity of the lens (Einstein 1936). The phenomenon causes splits and distortions of the source star image. For source stars located in the Milky Way Galaxy, the separation between the split images is of order milli-arcsecond and thus the individual images cannot be directly observed. However, the phenomenon can be photometrically observed through the brightness change of the source star caused by the change of the relative lens-source separation (Paczyński 1986). Since the first discovery in 1993 (Alcock et al. 1993; Udalski 1993), there have been numerous detections of microlensing events toward the Large and Small Magellanic Clouds, M31, and mostly the Galactic bulge fields. Currently, microlensing events are being detected at a rate of nearly 1000 events per year (Udalski 2008; Bond et al. 2001).

The properties of multiple systems such as binary frequency and mass function provide important constraints for star formation theories, enabling a concrete, qualitative picture of the birth and evolution of stars. At very low masses down to and below the hydrogen burning minimum mass, however, our understanding of formation processes is not clear due to the difficulties of observing these objects. Over the last decade, there have been several searches for very low mass binaries [see reviews by Basri (2000); Oppenheimer et al. (2000); Kirkpatrick (2005); Burgasser et al. (2007)]. Despite these efforts, the number of very low mass binaries[2] is not big enough to strongly constrain their formation processes.

Microlensing occurs regardless of the brightness of lens objects and thus it is potentially an effective method to investigate the mass function of low-mass binaries. For lensing events caused by single-mass objects, it is difficult to measure the lens mass because the Einstein time scale t_E, which is the only observable that provides information about the lens for general lensing events, results from the combination of the mass and distance to the lens and the transverse speed between the lens and source. The degeneracy can be partially lifted by measuring either an Einstein radius or a lens parallax and can be completely broken by measuring both. Einstein radii are measured from the deviation in lensing light curves caused by the finite-source effect (Gould 1994). Most microlensing events produced by binaries are identified from the anomalies involved with caustic approaches or crossings during which the finite-source effect is important (Nemiroff & Wickramasinghe 1994; Witt & Mao 1994). Therefore, Einstein radii can be routinely measured for the majority of binary-lens events. The microlens parallax is defined by

$$\pi_E = \frac{\pi_{rel}}{\theta_E}, \qquad (1)$$

PO Box 339, Bloemfontein 9300, South Africa.
[37]Lawrence Livermore National Laboratory, IGPP, PO Box 808, Livermore, California 94551, USA
[38]Centre for Star and Planet Formation, Geological Museum, Øster Voldgade 5-7, 1350 Copenhagen, Denmark.
[39]Corresponding author

[2] An updated list of binaries with total masses below 0.2 $M_\odot$ can be found at the "Very-Low-Mass Binary Archive" (http://ldwarf.ipac.caltech.edu/vlm/), and contains 99 entries as of Jan. 2010.

where $\pi_{rel} = AU(D_L^{-1} - D_S^{-1})$ is the lens-source relative parallax and D_L and D_S are the distances to the lens and source, respectively. In general, parallaxes can be measured for events that last long enough that the Earth's motion can no longer be approximated as rectilinear during the event (Gould 1992). The chance to measure the lens parallax for binary-lens events is higher than that of single-lens events because the average mass of binaries is bigger and thus time scales tend to be longer. In addition, the well-resolved caustic-crossing part of lensing light curves provide strong constraints on the lensing parameters and thus helps to pin-down enough anchor points on the light curve to extract otherwise too-subtle parallax effects (An & Gould 2001).

The number of binary-lens events with well-resolved anomalies is increasing with the advance of observational strategies such as the alert system and follow-up observations. The increase of the monitoring cadence of existing and planned survey experiments will make the detection rate even higher. Although binary microlensing is biased toward separations similar to the Einstein radius, it is easily quantifiable for next-generation experiments that have continuous "blind" monitoring. Therefore, microlensing will be able to provide an important method to discover very low mass binaries and to investigate their mass function.

In this paper, we present the microlensing discovery and characterization of a very low mass binary. We use this discovery to demonstrate that microlensing will provide a method to measure the mass function of very low-mass binaries that is free from the biases and difficulties of traditional methods.

3. OBSERVATIONS

The low-mass binary was detected from observations of the microlensing event OGLE-2005-BLG-153. The event occurred on a Galactic bulge star located at right ascension $\alpha = 18^h04^m17^s.30$ and declination $\delta = -28°40'49''.3$ (J2000), which corresponds to the Galactic coordinates $(l, b) = (2.3°, -3.4°)$. The event was detected by the Optical Gravitational Lensing Experiment (OGLE) using the 1.3 m Warsaw telescope of Las Campanas Observatory in Chile and was announced as a probable microlensing event on 14 April 2005. The event was independently identified by the Microlensing Observation in Astrophysics (MOA) as MOA-2005-BLG-023 using the 0.6 m of Mt. John Observatory in New Zealand.

An anomaly alert was issued on 3 July 2005 by the Probing Lensing Anomalies Network (PLANET) collaboration. Following the alert, the PLANET, RoboNet, and Microlensing Follow-Up Network (μFUN) teams intensively observed the event by using eight telescopes located on three different continents. These telescopes include the PLANET 1.54 m Danish Telescope of La Silla Observatory in Chile, PLANET 1.0 m of Mt. Canopus Observatory in Australia, PLANET 0.6 m of Perth Observatory in Australia, μFUN 1.3 m SMARTS telescope of CTIO in Chile, RoboNet 2.0 m Faulkes Telescope S. (FTS) in Australia, RoboNet 2.0 m Faulkes Telescope N. (FTN) in Hawaii, and RoboNet 2.0 m Liverpool Telescope (LT) in La Palma, Spain. Thanks to the follow-up observations, the light curve was densely resolved.

The event was analyzed before by Skowron et al. (2007) based on the data from OGLE observations as one of 9 binary-lens events detected in 2005 season. Here we reanalyze the event in depth with the addition of data from follow-up observations focusing on the physical parameters of the lens system.
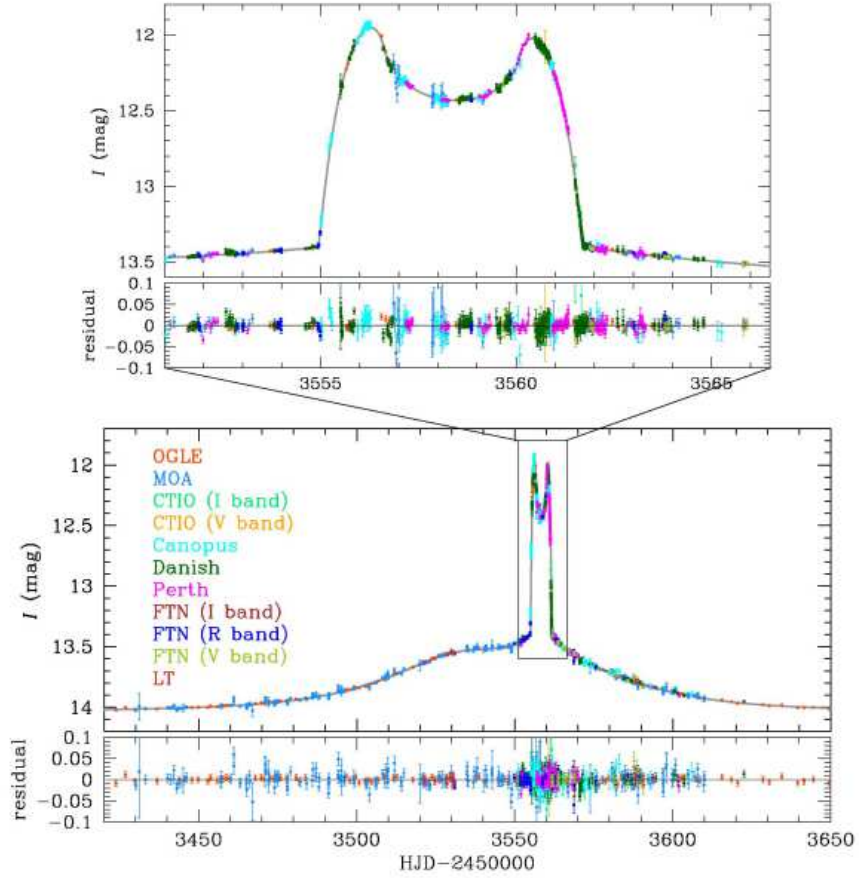
FIG. 1.— Light curve of the microlensing event OGLE-2005-BLG-153. Also presented is the model curve for the best-fit solution. The upper panel shows a zoom of the caustic-induced perturbation region.

4. MODELING

Figure 1 shows the light curve of the event. It is characterized by the sharp rise and fall occurring at around the heliocentric Julian dates (HJD) of 2453556 and 2453560. These features are caused by the crossings of the source star across a caustic, which represents a set of source positions at which the lensing magnification of a point source becomes infinite. Therefore, the existence of such a feature immediately reveals that the lens is composed of two masses (Mao & Paczyński 1991).

Characterization of binary lenses requires modeling of lensing light curves. We test 3 different models. In the first model, we test a static binary model (standard model). In this model, the light curve is characterized by 7 parameters. The first set of three parameters are needed to describe the light curves of single-lens events: the time required for the source to transit the Einstein radius, t_E (Einstein time scale), the time of the closest lens-source approach, t_0, and the lens-source separation in units of the Einstein radius at the time of t_0, u_0 (impact parameter). Another set of three parameters are needed to describe the deviation caused by the lens binarity: the projected binary separation in units of the Einstein radius, s, the mass ratio between the binary components, q, and the angle of the source trajectory with respect to the binary axis, α (source trajectory angle). Finally, an additional parameter of the ratio of the source radius to the Einstein radius, $\rho_\star = \theta_\star/\theta_E$ (normalized source radius), is needed to incorporate the deviation of the light curve caused by the finite-source effect. In the sec-

ond model, we consider the parallax effect by including two additional parallax parameters of $\pi_{E,N}$ and $\pi_{E,E}$, which are the two components of the microlensing parallax vector $\boldsymbol{\pi}_E$ projected on the sky in the direction of north and east celestial coordinates. In the last model, we additionally check the possibility of the effect on the lensing light curve caused by the orbital motion of the lens. The orbital motion affects the lensing magnifications in two different ways. First, it causes the binary axis to rotate or, equivalently, makes the source trajectory angle change in time. Second, it causes the separation between the lens components to change in time. The latter effect causes alteration of the caustic shape in the course of an event. To first order, the orbital effect is parameterized by

$$\alpha(t) = \alpha(t_0) + \omega \left(\frac{t - t_0}{t_E} \right) \qquad (2)$$

and

$$s(t) = s(t_0) + \dot{s} \left(\frac{t - t_0}{t_E} \right) \qquad (3)$$

where the orbital parameters ω and $\dot{s}$ represent the rates of change of the source trajectory angle and the projected binary separation, respectively. Considering the orbital effect is important not simply to constrain the orbital motion of the lens system but also to precisely determine the lens mass. This is because both the motions of the observer (parallax effect) and the lens (orbital effect) have a similar effect of causing deviations of the source trajectory from a straight line. Then,

	standard	parallax		parallax+orbit	
		$(u_0 > 0)$	$(u_0 < 0)$	$(u_0 > 0)$	$(u_0 < 0)$
χ^2	2406.812	1836.199	1982.545	**1672.572**	1674.966
t_0 (HJD')	3549.8286±0.0556	3551.2263±0.0950	3549.4179±0.0692	**3549.1650±0.0992**	3548.6344±0.1452
u_0	0.502±0.002	0.481±0.003	-0.515±0.002	**0.566±0.003**	-0.572±0.004
t_E (days)	46.428±0.111	48.735±0.149	50.019±0.229	**44.541±0.121**	44.952±0.173
s	0.837±0.001	0.836±0.001	0.832±0.001	**0.848±0.001**	0.847±0.001
q	0.848±0.003	0.848±0.003	0.833±0.003	**0.871±0.003**	0.865±0.002
α	5.902±0.001	5.956±0.003	0.373±0.003	**5.900±0.002**	0.396±0.003
$\rho_\star$	0.017±0.001	0.017±0.001	0.016±0.001	**0.018±0.001**	0.018±0.001
Γ_I	0.571±0.019	0.510±0.016	0.545±0.016	**0.501±0.014**	0.495±0.013
$\pi_{E,N}$		0.762±0.040	0.555±0.078	**0.106±0.047**	0.196±0.175
$\pi_{E,E}$		0.699±0.031	0.921±0.042	**0.419±0.031**	0.385±0.029
$\dot{s}$				**-0.0651±0.0020**	-0.0693±0.0022
$\dot{\alpha}$				**0.0064±0.0068**	-0.0004±0.0101

NOTE. — HJD' = HJD − 2450000. The parameters of the best-fit model are marked in bold font.

if the orbital motion of the lens is not considered despite its non-negligible effect, the deviation of the lensing light curve caused by the orbital effect may be explained by the parallax effect. This will cause a wrong determination of the lens parallax and the resulting lens mass.

When either the effect of the parallax or orbital motion is considered, a pair of source trajectories with impact parameters $u_0 > 0$ and $u_0 < 0$ result in slightly different light curves due to the breakdown of the mirror-image symmetry of the source trajectory with respect to the binary axis. We, therefore, check both models with $u_0 > 0$ and $u_0 < 0$ whenever the parallax or orbital effect is considered. As a result, the total number of tested models is 5.

To find the best-fit solution of the lensing parameters, we use a combination of grid and downhill approaches. It is difficult to find solutions from pure brute-force searches because of the sheer size of the parameter space. It is also difficult to search for solutions from a simple downhill approach because the χ^2 surface is very complex and thus even if a solution that apparently describes an observed light curve is found, it is hard to be sure that all possible χ^2 minima have been searched. To avoid these difficulties, we use a hybrid approach in which a grid search is conducted over the space of a subset of parameters (grid parameters) and the remaining parameters are searched by a down-hill approach to yield minimum χ^2 at each grid point. Then, the best-fit solution is found by comparing the χ^2 values of the individual grid points. We set s, q, and α as grid parameters because they are related to the features of light curves in a complicated pattern while other parameters are more directly related to the identifiable light curve features. For the down-hill χ^2 minimization, we use a Markov Chain Monte Carlo method.

5. RESULTS

In Table 1, we present the results of modeling along with the best-fit parameters for the individual models. It is found that the effects of parallax and orbital motion are needed to precisely describe the light curve. We find that the model with the parallax effect improves the fit by $\Delta\chi^2 = 571$. The fit further improves by $\Delta\chi^2 = 164$ with the addition of the orbital effect. We note that the values of the parallax parameters from the "parallax+orbit" model are different from those determined from the "parallax" model. This demonstrates that consideration of the orbital effect is important for the precise measurement of the lens parallax.
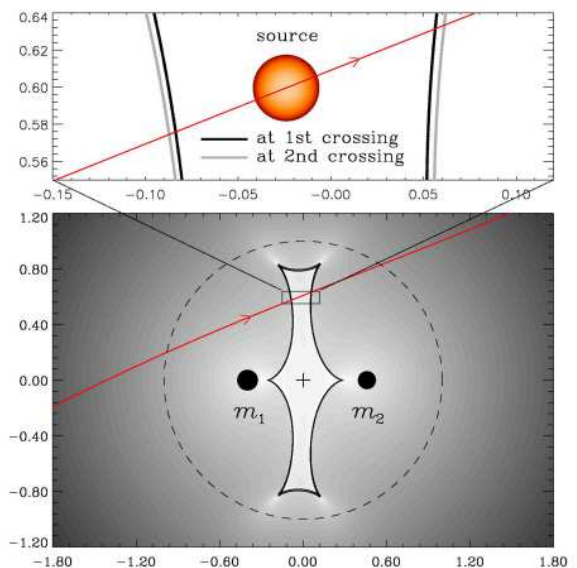

FIG. 2.— Geometry of the binary lens system responsible for the lensing event OGLE-2005-BLG-153. In the lower panel, the two filled dots represent the locations of the binary lens components. The dashed circle is the Einstein ring corresponding to the total mass of the binary. The ring is centered at the center of mass of the binary (marked by '+'). The line with an arrow represents the source trajectory. We note that the trajectory is curved due to the combination of the effects of parallax and lens orbital motion. The closed figure composed of concave curves represents the positions of the caustic formed by the binary lens. All lengths are normalized by the Einstein radius. The temperature scale represents the magnification where brighter tones imply higher magnifications. The upper panel shows a zoom of the boxed region. We note that the caustic shape slightly changes due to the orbital motion of the lens. We present the caustics at the two different moments of the caustic entrance and exit of the source star.

In Figure 1, we present the model light curve on the top of observed data points. Figure 2 shows the geometry of the lens system corresponding to the best-fit solution, i.e. "parallax+orbit" model with $u_0 > 0$. In the figure, the filled dots represent the locations of the binary components, the dashed circle is the Einstein ring corresponding to the total mass of the lens, the closed figure composed of concave curves is the caustic formed by the lens, and the curve with an arrow represents the source trajectory. The upper panel shows an enlargement of the region where the source trajectory crosses the caustic. The shape of the caustic changes in time due to
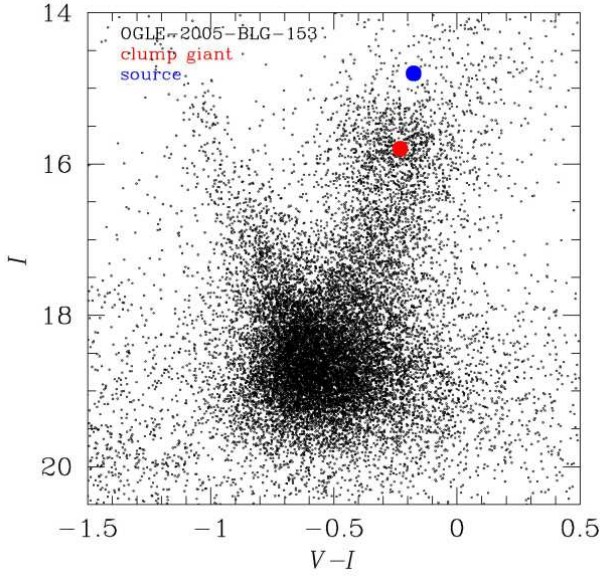
FIG. 3.— Positions of the source (lensed) star with respect to the centroid of clump giants in the instrumental color-magnitude diagram.

the orbital motion of the lens, and thus we present the caustics at two different moments of the caustic entrance and exit of the source star.

Among the two quantities needed for the determination of the lens mass, the microlens parallax is obtained directly from the parallax parameters determined from modeling by

$$\pi_E = \left(\pi_{E,N}^2 + \pi_{E,E}^2\right)^{1/2} = 0.432 \pm 0.042. \qquad (4)$$

On the other hand, the Einstein radius is not directly obtained from modeling. Instead, it is inferred from the normalized source radius $\rho_\star$, which is determined from modeling, combined with the information about the angular source radius $\theta_\star$. The angular source radius is determined from the information of the de-reddened color of the source star measured by using the centroid of clump giant stars in the color-magnitude diagram as a reference position under the assumption that the source and clump centroid experience the same amount of extinction (Yoo et al. 2004). Figure 3 shows the instrumental color-magnitude diagram constructed based on CTIO V and I band images and the locations of the source star and the centroid of clump giants. By measuring the offsets in the color and magnitude between the source and the centroid of clump giants combined with the known color and absolute magnitude of the clump centroid of $[(V-I), M_I]_c = (1.04, -0.25)$, we estimate that the de-reddened magnitude and color of the source star are $I_0 = 13.16$ and $(V-I)_0 = 1.09$, respectively, implying that the source is a clump giant with an angular radius of $\theta_\star = 11.72 \pm 1.01$ μas. Here we adopt a Galactocentric distance of 8 kpc and the offset of the bar of the field is 0.4 kpc toward the Sun and thus the distance to the clump centroid is 7.6 kpc based on the Galactic model of Han & Gould (2003). Then, with the measured normalized source radius of $\rho_\star = 0.018 \pm 0.001$, the Einstein radius is estimated as

$$\theta_E = \frac{\theta_\star}{\rho_\star} = 0.66 \pm 0.06 \text{ mas.} \qquad (5)$$

Together with the Einstein time scale, the relative lens-source proper motion is obtained by $\mu = \theta_E/t_E = 5.38 \pm 0.47$ mas yr^{-1}.

With the measured Einstein radius and lens parallax, the

mass of the lens system is uniquely determined by

$$m = \frac{\theta_E}{\kappa \pi_E} = 0.19 \pm 0.02 \, M_\odot, \qquad (6)$$

where $\kappa = 4G/(c^2 \text{AU})$. With the known mass ratio between the binary components, the masses of the individual binary components are determined, respectively, as

$$m_1 = \frac{1}{1+q} m = 0.10 \pm 0.01 \, M_\odot \qquad (7)$$

and

$$m_2 = \frac{q}{1+q} m = 0.09 \pm 0.01 \, M_\odot. \qquad (8)$$

This implies that both lens components are very low mass stars with masses just above the hydrogen-burning limit of $0.08 \, M_\odot$. The distance to the lens is determined as

$$D_L = \frac{\text{AU}}{\pi_E \theta_E + \pi_S} = 2.42 \pm 0.21 \text{ kpc}, \qquad (9)$$

where $\pi_S = \text{AU}/D_S$ is the parallax of the source star. From this distance to the lens combined with the Einstein radius, it is found that the two low-mass binary components are separated with a projected separation of

$$r_\perp = s D_L \theta_E = 1.35 \pm 0.12 \text{ AU}. \qquad (10)$$

It is also found that the lens velocity in the frame of the local standard of rest is $\mathbf{v} = (v_\perp, v_\parallel) = (-20.9 \pm 31.9, 15.1 \pm 31.9)$ km s^{-1}, where $v_\perp$ and $v_\parallel$ are the velocity components normal to and along the Galactic plane, respectively. We note that the errors in v are dominated by the unknown proper motion of the source, which is assumed to be 0 ± 100 km s^{-1} in the Galactic frame. The velocity and the distance to the lens imply that the lens is in the Galactic disk.

In addition to the parallax effect, the relative lens-source motion can, in principle, also be affected by the orbital motion of the source star if it is a binary (Smith, Mao, & Paczyński 2003). We check the possibility that this so-called "xallarap" (reverse of "parallax") effect influences the parallax determination. For this, we conduct additional modeling including the xallarap effect. For the description of the xallarap effect, 3 additional parameters of the phase angle, inclination, and orbital period are needed under the assumption that the source moves in a circular orbit. From this analysis, we find that the xallarap effect does not provide a better model than the parallax model. In addition, the best-fit occurs for an orbital period of ~ 1 yr, which corresponds to the orbital period of the Earth around the Sun. Furthermore, the best-fit values of the inclination and the phase angle are similar to the ecliptic longitude and latitude of the source star. All these facts imply that the xallarap interpretation of the light-curve deviation is less likely and support the parallax interpretation (Poindexter et al. 2005; Dong et al. 2009).

From the orbital parameters ω and $\dot{s}$ determined from modeling along with the assumption of a circular orbit, one can obtain the usual orbital parameters of the semi-major axis, a, orbital period, P, and inclination, i, of the orbit of the binary lens from the relations

$$a = \frac{r_\perp}{x}; \qquad P = \left(\frac{a^3}{m}\right)^{1/2}; \qquad \cos i = -(xB)^{1/2}. \qquad (11)$$

Here $B = r_\perp^3 \omega^2/(Gm)$, $x = \sin \phi$, and ϕ is the angle between the vector connecting the binary components and the line of

sight to the lens such that the projected binary separation is $r_\perp = a\sin\phi$. The value of x is obtained by solving the equation $x^3 - Bx^2 - x + (A^2 + 1)B = 0$, where $A = (\dot{s}/s)/\omega$ (Dong et al. 2009). We find that the semi-major axis is $a = 1.46 \pm 0.08$ AU and the period is $P = 4.05 \pm 0.19$ yrs. The inclination of the orbital plane is $i = 88.3° \pm 1.1°$, implying that the orbit is very close to edge on.

We can also constrain the surface brightness profile of the source star by analyzing the caustic-crossing parts of the light curve. We model the source brightness profile as

$$S_\lambda = \frac{F}{\pi\theta_\star^2}\left[1 - \Gamma_\lambda\left(1 - \frac{3}{2}\cos\theta\right)\right], \qquad (12)$$

where Γ_λ is the linear limb-darkening coefficient and θ is the angle between the normal to the stellar surface and the line of sight toward the source star, and F is the source flux. We measure the coefficient in I band of $\Gamma_I = 0.501 \pm 0.014$. The measured coefficient is consistent with the theoretical value of clump giants (Claret 2000).

6. DISCUSSION AND CONCLUSION

We analyze the light curve of a binary-lens microlensing event OGLE-2005-BLG-153, which exhibits a strong caustic-crossing structure on the light curve. By measuring both the Einstein radius and the lens parallax, we could uniquely measure the masses of the individual lens components. The measured masses were $0.10 \pm 0.01\ M_\odot$ and $0.09 \pm 0.01\ M_\odot$, respectively, and thus the binary was composed of very low-mass stars just above the hydrogen-burning limit.

Although the event OGLE-2005-BLG-153 is one of few cases with well-measured lens masses among the 5000 microlensing events discovered to date, the event characteristics that enabled this mass measurement are likely to become common as next-generation microlensing experiments come

on line. Because next-generation experiments will provide intense coverage from sites on several continents, most caustic-crossing binaries will yield masses. Moreover, because next-generation cadences will be independent of human intervention, rigorous characterization of the selection function will be straightforward. Finally, for reasonable extrapolations of the mass function of stars close to and below the hydrogen-burning limit, we can anticipate an important fraction of the roughly thousand events per year expected to be detected from next-generation surveys to be due to low-mass objects including brown dwarfs (Gould 2009). Hence, the mass function, at least of objects within binaries, will be measurable for all Galactic populations of low-mass stellar and substellar objects in the near future, independent of biases caused by the luminosity of the population.

REFERENCES

Alcock, C., et al. 1993, Nature, 365, 621
An, J., & Gould, A. 2001, ApJ, 563, L111
Aubourg, E., et al. 1993, Nature, 365, 623
Basri G. 2000, ARA&A, 38, 485
Bond, I. A., et al. 2002, MNRAS, 333, 71
Burgasser, A. J., et al. 2007, Protostars and Planets V, (B. Reipurth eds.), University of Arizona Press, Tucson, 427
Claret, A. 2000, A&A, 363, 1081
Dong, S., et al. 2009, ApJ, 695, 970
Einstein, A. 1936, Science, 84, 506
Gould, A. 1992, ApJ, 392, 442
Gould, A. 1994, ApJ, 421, L71
Gould, A. 2009, ApJ, 698, L147
Han, C., & Gould, A. 2003, ApJ, 592, 172

Kirkpartrick, J. D. 2005, ARA&A, 43, 195
Mao, S., & Paczyński, B. 1991, ApJ, 374, L37
Nemiroff, R. J., & Wickramasinghe, W. A. D. T. 1994, ApJ, 424, L21
Oppenheimer B. R., Kulkarni S. R., & Stauffer J. R. 2000, Protostars and Planets IV (V. Mannings et al., eds.) Univ. of Arizona, Tucson, 1313
Paczyński, B. 1986, ApJ, 308, L43
Poindexter, S., et al. 2005, ApJ, 633, 914
Skowron, J. S., et al. 2007, Acta Astron., 57, 281
Smith, M. C., Mao, M., & Paczyński, B. 2003, MNRAS, 339, 925
Udalski, A., et al. 1993, Acta Astron., 58, 69
Udalski, A., Szymański, M. K., Soszyński, I., and Poleski, R. 2008, Acta Astron., 58, 69
Witt, H. J., & Mao, S. 1994, ApJ, 430, 505
Yoo, J., et al. 2004, ApJ, 603, 139